Supplementary information

Variation of fluorescent intensity

Variations of the *x*-directional profile of the normalized fluorescence intensity in a rectangular region of interest (ROI) of 1280 pixel ×148 pixel (1,113 μm × 129 μm) between PDMS posts in the gel region for 70 kDa dextran under normoxia and hypoxia are shown in Fig. S1. These figures correspond to the microscope images in Fig. 2(a). The intensity in the gel ($x \leq 0$ mm) gradually increases, while that in the media channel ($x > 0$ mm) is constant at 1. The intensity profile under normoxia saturates 2 hours after the dextran infusion, and a quasi-steady state of dextran diffusion is generated (Fig. S1(a)). In contrast, the amount of change in the intensity profile is fluctuating under hypoxia, indicating transition of the integrity of EC monolayer (Fig. S1(b)).

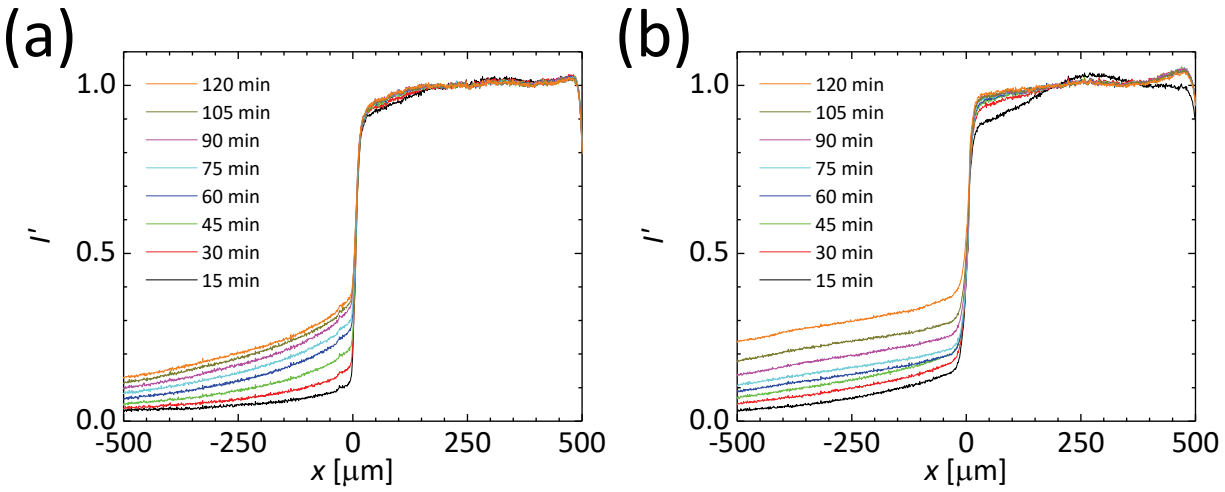

Fig. S1 Transient changes of the *x*-directional profile of the normalized fluorescence intensity *I'* in a ROI for 70 kDa dextran after the injection under (a) normoxia and (b) hypoxia.

Steady-state analysis for endothelial permeability

In the former studies,[1, 2] permeability of the EC monolayer was quantified based on the balance of flux of the dextran through the EC monolayer, assuming a steady-state condition:

$$P = \beta D \frac{dC/dx}{\Delta C_{ec}} \quad \text{(S1)}$$

where dC/dx is the gradient of dextran concentration in collagen gel, ΔC_{ec} is the concentration difference across the EC monolayer, β (= 1 in the present study) is the correction factor reflecting the change of the cross-sectional area of the gel, and D is the diffusion coefficient of the dextran in the gel.

In the calculation of the permeability by Eq. (S1), the diffusion coefficient D was unknown. Hence, the value D was estimated by comparing experimental data with computational result. We conducted the above-mentioned time-lapse observations of diffusions of 70 kDa and 10 kDa fluorescent dextrans in the microfluidic device without cells, as well as

3D unsteady numerical simulations of the diffusion of dextran by employing commercial finite element software (COMSOL Multiphysics 4.4, COMSOL, USA). In the computation, the 3D geometry of the gel channel was reconstructed and discretized into ~11×10^6 elements. Boundary conditions of normalized concentrations of 1 and 0 were applied on the right and left gel surfaces, respectively. Zero flux conditions were imposed on the PDMS and glass surfaces. The diffusion coefficient of each dextran was estimated by means of the golden section search,[3] in which the error between experimental and computational profiles of the dextran concentration was minimized. More specifically, the *y*-directional averaged concentration profiles for -420 μm ≤ x ≤ -20 μm in the gel in the above-mentioned ROI after 15 min of dextran diffusion were used for the evaluation. The search ranges were set between 2.0×10^{-11} m^2/s and 5.0×10^{-11} m^2/s for 70 kDa dextran and between 7.0×10^{-11} m^2/s and 1.0×10^{-10} m^2/s for 10 kDa dextran, and the convergence criterion was set at 0.01×10^{-11} m^2/s for both cases. To determine the diffusion coefficients of the two dextrans, two gel regions were measured in each of three microfluidic devices, and the averaged profiles were compared with computational results.

An example of a fluorescent microscope image obtained 15 min after the injection of 70 kDa fluorescent dextran is shown in Fig. S2(a). The fluorescence intensity of the gel region gradually increased toward the left-hand side, whereas that in the media channel remained approximately constant at a high intensity. Numerical simulations performed over a range of diffusion coefficients with the golden section search agreed most closely with the experimental dextran concentration distribution using a value $D = 4.0\times10^{-11}$ m^2/s (Fig. S2(b)). As observed in the comparison between Figs. S2(a) and (c), the computed distribution of the dextran is similar to the measured one. In the same way, the diffusion coefficient of 10 kDa dextran was also estimated as $D = 9.2\times10^{-11}$ m^2/s (Fig. S2(b)). Quantitative agreements of distributions of dextrans between measurement and computation are confirmed in Fig. 2(d). In former studies,[1, 2] similar values for the diffusion coefficients of 70 kDa and 10 kDa dextrans were estimated based on the scale law as 4.5×10^{-11} m^2/s and 9.0×10^{-11} m^2/s, respectively. The slight deviances of the values between the present and former studies might be due to different concentrations and/or pH level of the collagen gel.

Numerical simulation revealed changes of dextran concentration profile across the gel channel. Dextran concentration profiles nondimensionalized with the diffusion coefficient D and the width of the gel channel L are shown in Fig. S2(e). When nondimensionalized time tD/L^2 was one, dextran concentration inside the gel almost reached the steady state. Dextran concentration at the center of the gel channel (x/L = -0.5) approached 0.5 as shown in Fig. S2(f). For 70k Da and 10 kDa dextrans, the observation time point of 2 hours corresponded to tD/L^2 = 0.17 and 0.39, respectively.

Permeability values of each EC monolayer for 70 kDa and 10 kDa dextrans are compared between transient analysis and steady-state analysis methods (Fig. S3). The value of dC/dx in Eq. (S1) was quantified in the range of -500 μm ≤ x ≤ -200 μm in each ROI. The two methods provide almost the same permeability values without a statistical significance for

each condition. The significant differences between the results under normoxia and hypoxia are confirmed also in the steady-state analysis result.

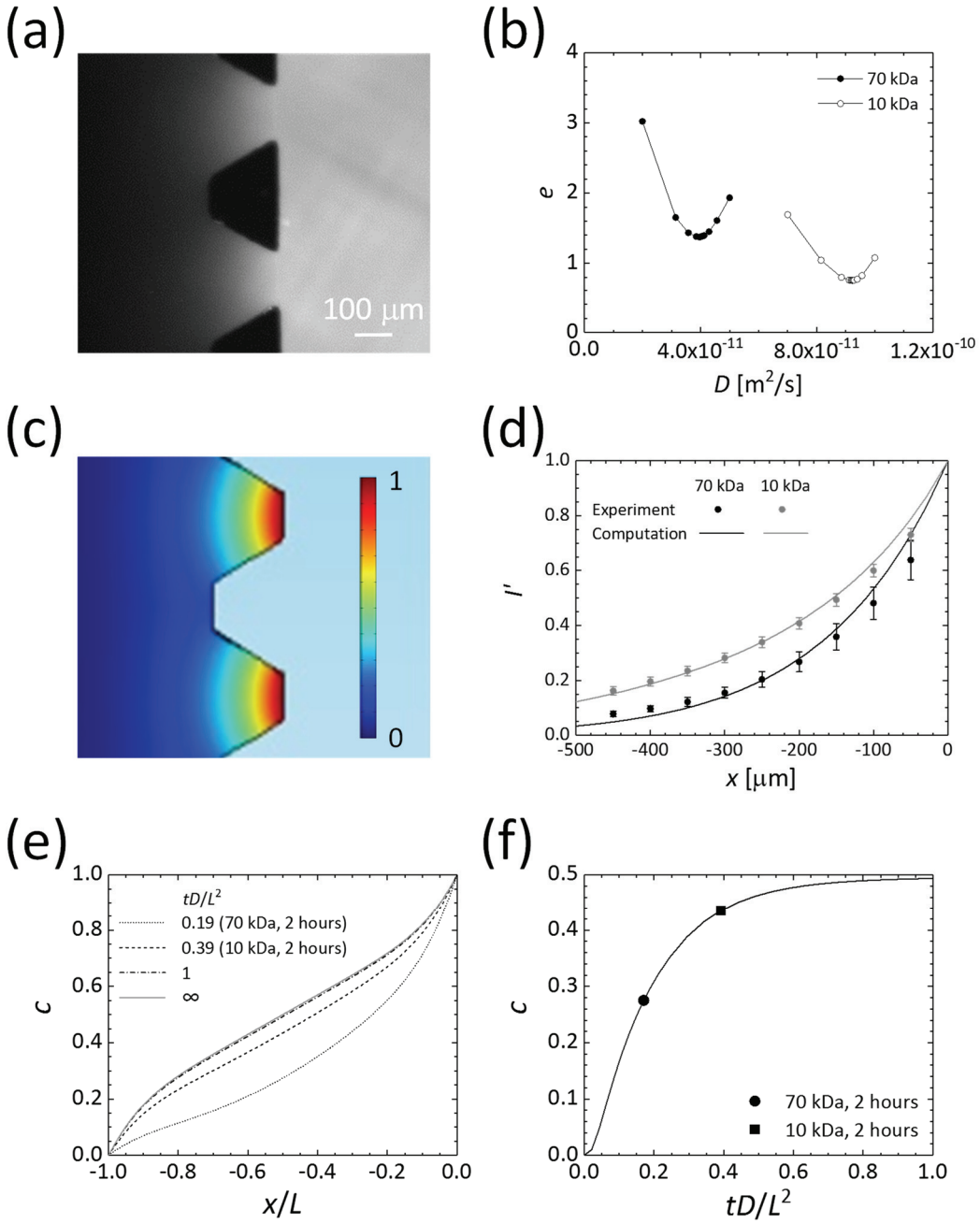

Fig. S2 Diffusion of fluorescent dextrans of 70 kDa and 10 kDa in collagen type I gel of 2.5 mg/ml. (a) A fluorescent microscope image of the fluorescent dextran of 70 kDa after 15 min of the infusion of the dextran solutions into the media channel. (b) Normalized errors e of fluorescence intensities in ROI between experiment and computation in the golden section search of diffusion coefficients of 70 kDa and 10 kDa dextrans. (c) A computational result of normalized concentration c of dextran with the diffusion coefficient of $D = 4.0\times10^{-11}$ m^2/s after 15 min of the infusion. (d) Comparisons of normalized fluorescence intensity I' (or concentration c) profiles between experimental data for the dextrans of 70 kDa and 10 kDa and computational results for 4.0×10^{-11} m^2/s and 9.2×10^{-11} m^2/s, respectively. Error-bars represent standard deviation. (e) Profiles of dextran concentration along the x-direction, nondimensionalized with the width L (1,300 μm) of the gel channel. (f) Variation of dextran concentration at the center of the gel channel ($x/L = -0.5$) with nondimensionalized time tD/L^2.

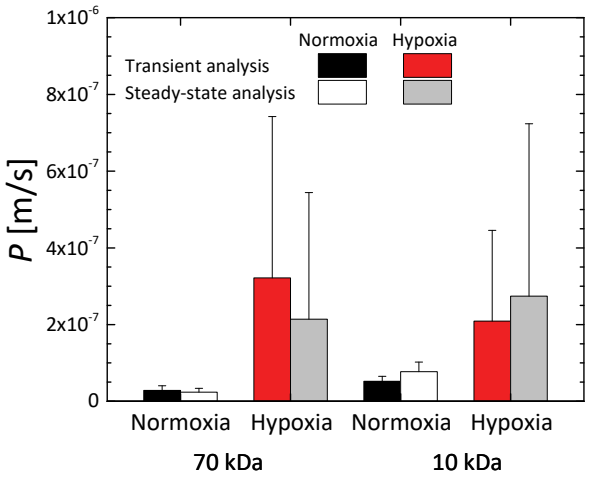

Fig. S3 Comparison of permeability values P between two methods of the present transient analysis and the former steady-state analysis. Error-bars represent standard deviation.

Endothelial monolayer on a vertical gel surface in the microfluidic device

Morphological changes of HUVECs were observed by immunofluorescent imaging after the 6-hour normoxic or hypoxic exposure in the microfluidic device. The confocal microscope images of HUVECs on the gel surface of 150 μm height were taken at an interval of 0.63 μm in the z-direction. Maximum intensity projections of the images of HUVECs to the zy-plane (a gel surface) were then obtained by image processing as shown in Fig. S4. Similar to HUVECs on the glass cover slip, VE-cadherin around HUVECs on the gel surface are observed as thick bands under normoxia. On the other hand, they are somewhat indistinct under hypoxia.

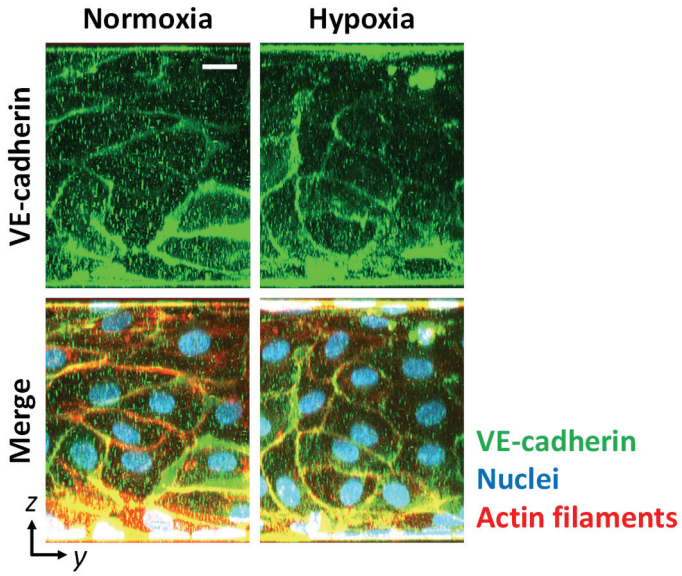

Fig. S4 Maximum intensity projections of confocal microscope images of HUVECs to the zy-plane (the gel surface) after the normoxic or hypoxic exposure. VE-cadherin, nuclei, and actin filaments were stained with green, blue, and red, respectively. Scale bar represents 20 μm.

Morphology of endothelial cells

The HUVEC morphology under each oxygen condition was evaluated, assuming an elliptical shape. The aspect ratio of HUVECs as well as the angle of the major axis against the *x*-direction are plotted in Fig. S5, showing a wide variety of cell shapes. The aspect ratios under normoxia and hypoxia were 0.58 ± 0.16 and 0.52 ± 0.20, respectively. The angles were 101.68 ± 40.6 and 101.40 ± 46.09 for normoxic and hypoxic conditions, respectively. Neither metric showed significant difference between the two oxygen conditions, indicating that morphologies of HUVECs are similar under normoxia and hypoxia.

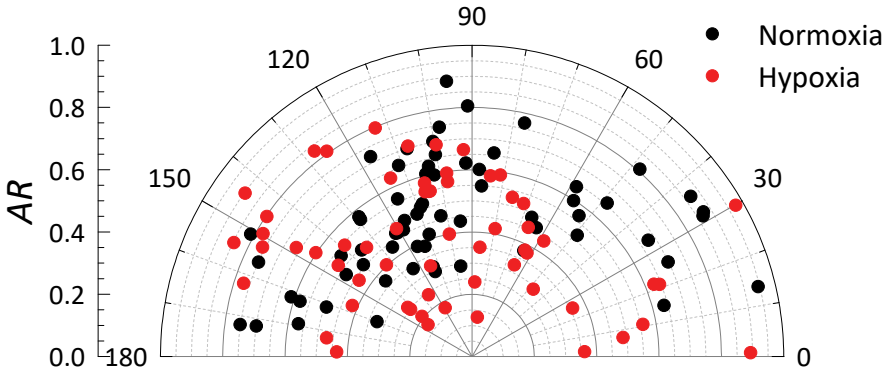

Fig. S5 Polar plotting of the aspect ratio *AR* of HUVECs under normoxia and hypoxia with the angle of the major axis against the *x*-direction. Those metrics were measured for the same cells evaluated in Fig. 4 (66 cells and 60 cells from three devices under normoxia and hypoxia, respectively).

Evaluation of tight junction around HUVECs

HUVECs were fixed and stained after the 6-hour normoxic or hypoxic exposure in the microfluidic device, following the protocol described in the subsection of Immunofluorescent imaging. Instead of VE-cadherin, ZO-1 was labeled with mouse monoclonal antibody (33-9100, Thermo Fisher Scientific, USA) at a dilution of 1:100 for 30 min, followed by staining with Alexa Fluor 488-conjucated secondary antibody (A110001, Life Tech, USA) at a dilution of 1:100 for 30 min. Confocal imaging showed no distinct difference between confocal images obtained 6-hour normoxic and hypoxic exposure as shown in Fig. S6(a).

In addition, protein level of ZO-1 was quantified by Western blot analysis of HUVECs cultured on cell culture dishes. Whole cell extraction was performed following the protocol described in the subsection of the Western blot analysis of HUVECs cultured on dish. Sodium dodecyl sulfate poly-acrylamide gel electrophoresis (SDS-PAGE) and transfer onto polyvinylidene difluoride (PVDF) of the proteins were conducted using 4-20% polyacrylamide gel (456-1093, Mini-Protean TGX gel, Bio-Rad, USA). For immunoblotting, the PVDF membranes were incubated in blocking buffer (1% BA and 0.05% Tween 20 in Tris-buffered saline (BA-TBS-T) with the above-mentioned anti-ZO-1 antibody at a 1:500 dilution and anti-β-actin antibody (sc-47778, Santa Cruz Biotechnology, USA) at a 1:400 dilution for 16 hours at 4°C, followed by

incubation in BA-TBS-T with anti-mouse IgG, HRP-linked antibody (7076, Cell Signaling Technology, USA) at a 1:2000 dilution for 1 hour at room temperature. Quantification results of ZO-1 protein level in HUVECs showed no significant difference between the two oxygen conditions (Figs. S6(b) and (c)).

In conclusion, the hypoxic condition did not cause a significant change to a tight junction of ZO-1 in the early stage of hypoxic exposure. These results agree with the reference.[4]

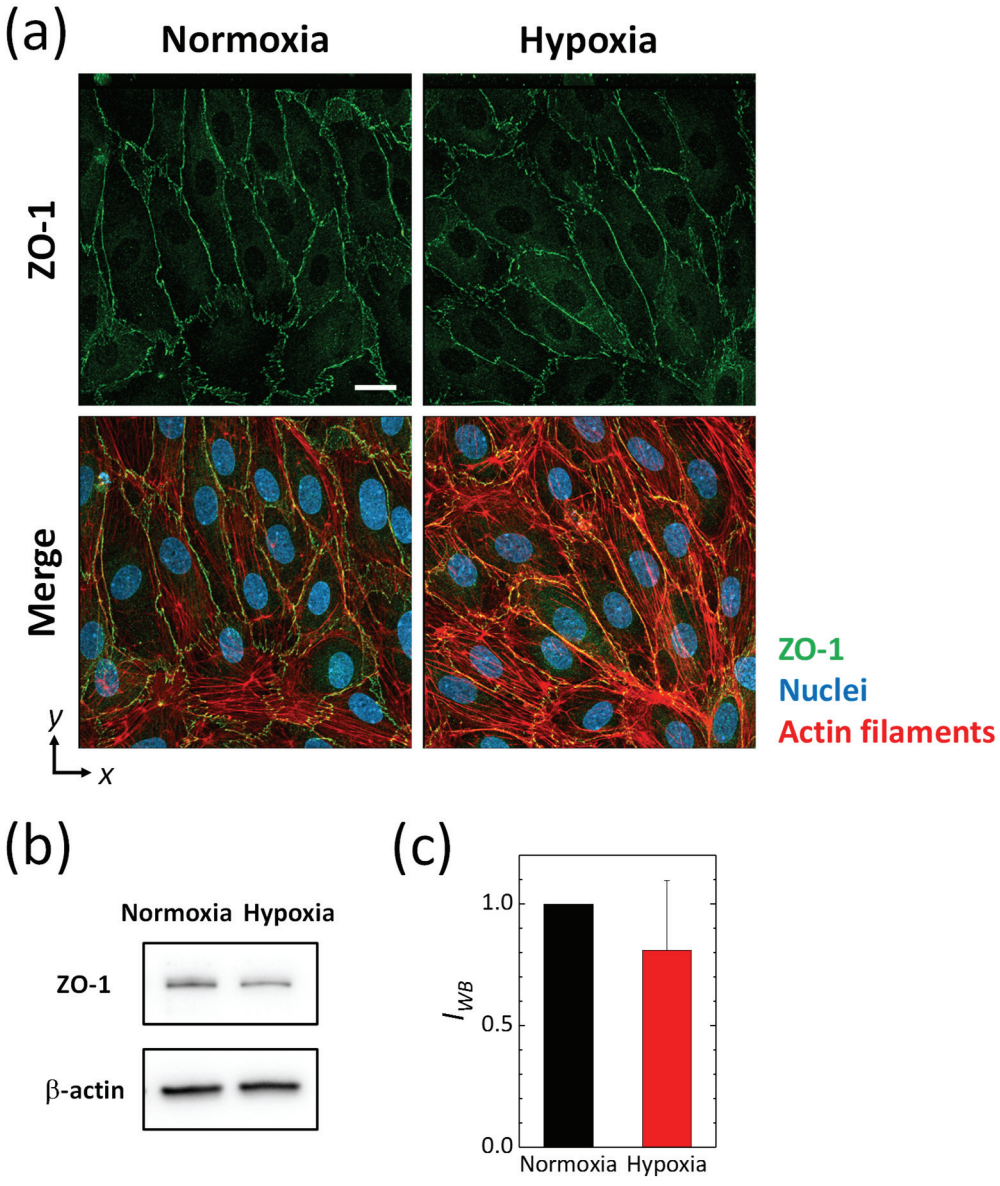

Fig. S6 Effect of 6-hour hypoxic exposure on ZO-1 of HUVECs. (a) Maximum intensity projections of confocal microscope images of HUVECs in microfluidic device to the *xy*-plane (the glass cover slip) after the normoxic or hypoxic exposure. Tight junction of ZO-1, nuclei, and actin filaments were stained with green, blue, and red, respectively. Scale bar represents 20 μm. (b) Representative bands of ZO-1 and β-actin by Western blotting of whole cell samples under normoxia and hypoxia, and (C) the normalized protein level I_{WB} of ZO-1 with the result of normoxia. The Western blot analysis of ZO-1 was conducted using HUVECs cultured on four cell culture dishes for each normoxic and hypoxic condition. Error-bar represents standard deviation.

References

1. I. K. Zervantonakis, S. K. Hughes-Alford, J. L. Charest, J. S. Condeelis, F. B. Gertler and R. D. Kamm, *Proc. Natl. Acad. Sci. U S A*, 2012, **109**, 13515-13520.
2. J. S. Jeon, I. K. Zervantonakis, S. Chung, R. D. Kamm and J. L. Charest, *PLoS One*, 2013, **8**, e56910.
3. W. H. Press, B. P. Flannery, S. A. Teukolsky and W. T. Vetterling, *Numerical recipes: the art of scientific computing*, University Press, Cambridge, 1986.
4. S. Engelhardt, A. J. Al-Ahmad, M. Gassmann and O. O. Ogunshola, *J. Cell. Physiol.*, 2014, **229**, 1096-1105.